



FAMU-FSU
Engineering

Understanding the Impact of Electrical Faults on High-Temperature Superconducting Power Cables for MVDC Power Systems of All-Electric Ships

Submitted as a Research Report for the Marshall Plan Foundation

By

Paul Mensah

26th January, 2023

Project supervisors

Professor Peter Cheetham

Professor Peter Zeller

Christoph Diendorfer

Professor Sastry Pamidi

Acknowledgments

I want to convey my deepest gratitude to Professor Peter Zeller for giving me the opportunity to join his experienced research team at FH Wels. Also, for his guidance, valuable input and feedback, and encouragement during this research opportunity in Austria.

I also want to thank Professor Sastry Pamidi, Professor Peter Cheetham, and Christoph Diendorfer for their continual support and commitment to ensuring this project went on smoothly. Their immense support from the conception of the project through the implementation and achieving the desired outcome never wavered.

I would also want to acknowledge Sebastian Gomez, Christian Gruberbauer, Romin Ramin, and Matthias Musil for their tremendous help and assistance during the research stay. Their methodical directions and insightful suggestions were of great help throughout the research.

Also, I would like to acknowledge the international offices of both FH Wels and Florida State University for their help and for making all this even possible.

Finally, I would like to thank the Austrian Marshall Plan Foundation for the scholarship, which gave me the opportunity to embark on this research exchange program to learn from the expertise of the host university and laboratory.

Table of Contents

Acknowledgments	2
Abstract.....	4
1. Introduction.....	5
1.1 Electrification of transportation.....	5
1.2 Background to superconductivity	5
2. Scientific question	12
3. High-Temperature Superconducting (HTS) power cables for electric transport applications	13
3.1 HTS Cable Designs.....	13
3.2 Choice of Cryogen	14
3.3 Cable Cryostat	15
3.4 Lapped Tape Insulation.....	15
4. Electrical Faults in HTS power cables of MVDC systems	21
4.1 Types of DC electrical Faults	21
4.2 Causes of parallel faults and their associated impact on power systems	22
4.3 Damage to the cryostat.....	22
5. Experimental Setup and Measurement Procedure.....	23
6. Results and Discussion	27
7. Conclusion	30
8. Appendix.....	31
9. List of figures	33
10. List of tables.....	34
11. References.....	35

Abstract

The goal of this project is to understand the effect of a parallel electrical fault on high temperature superconducting (HTS) power cables for medium voltage direct current (MVDC) power system for all-electric ships. Of particular interest is to understand how a pole-ground fault may cause physical damage to the associated cryogenic infrastructure required for HTS power cables. The experiments performed at FH Wels replicate similar geometries and materials which could be utilized by HTS power cables in electric ship applications. The findings of this study will support the design in terms of operating voltage and current of HTS cables for electric ship applications. Additionally, the results will give insight into HTS cable designs that will enhance the resiliency and stability of the power systems in electric transport systems to mitigate the effects of a pole-ground fault. A review of the background and principles of superconductivity is discussed. Different high-temperature superconducting cable designs were explored with their merits, demerits, and applications. Commonly used cryogens for HTS cables are discussed along with cable cryostats. Again, the different types of DC electrical faults, the causes and their associated impact on the power system are considered. The measurement was conducted for two different temperature ranges. That is, at room temperature and at cryogenic temperature of 77 K. The experimental setup and methodology are explained in detail. Finally, the results are discussed with conclusions established and suggestions made for future work.

1. Introduction

1.1 Electrification of transportation

The transportation sector is a major contributor to global greenhouse gas emissions, with the majority of emissions coming from the use of fossil fuels in cars, ships, and aircraft [1]–[3]. Electrifying transportation is crucial for reducing these emissions and mitigating the impacts of climate change. A significant amount of research over the years has gone into the electrification of different transport system applications to address the design constraints associated with combustion engines and the challenges with CO₂ emissions [4]–[6]. The development and implementation of electric vehicles have been rapid, widely popular, and accepted in the industry today. Several governmental agencies like the US Navy, National Aeronautics and Space Administration (NASA) and other private corporations are actively conducting research into all-electric aircraft and ships [7], [8]. Significant breakthroughs and progress has been made to achieve the required ambitious power density demands, power capacity targets, high efficiency and resiliency such all-electric power systems require. One of these breakthroughs is the use of high temperature superconducting (HTS) devices. The variable power ratings and high-power density of high temperature superconducting (HTS) devices makes it ideal and offer a far more potential solution for the power density and capacity challenges for electric transport applications [9]. The power demands for the electric ship and aircraft have been estimated to be 100 MW and 40 MW respectively [7], [10]. These power requirements are not possible to be realized using conventional copper cables without sacrificing the most important design criteria of transport applications, weight, and space [11]. HTS power cables have been installed in several terrestrial applications already to demonstrate its current carrying capability and other benefits [12]. Currently, superconducting power systems consisting of HTS generators, motors, and cables need to be developed with a holistic methodology to ensure the power system meets the electrical, cryogenic, and resiliency constraints it possesses [13].

1.2 Background to superconductivity

In 1911, a physicist named Kamerlingh Onnes was studying the electrical resistance of materials at cryogenic temperatures when he made the discovery of superconductivity. Onnes observed a strange phenomenon that was previously unknown when he decreased the temperature of mercury to 4 K and found that its electrical resistance quickly fell to zero. Onnes called this recently found characteristic superconductivity [14]. After that discovery, a number of materials have been shown to possess superconducting characteristics, with the earlier materials found prior to 1930 being classified as Type I materials [15]. This type of superconducting material loses its superconducting properties in the presence of weak magnetic fields. A different type of superconducting material was later discovered which could withstand strong magnetic fields before losing its superconducting property. This type of superconducting material is suitable for high-power applications. These were referred to as Type II materials. These two distinct materials could also be classified as low-temperature superconductors (LTS) and high-temperature superconductors (HTS). Niobium-titanium (NbTi) and niobium-tin (Nb₃Sn) are some examples of LTS, with bismuth-strontium-calcium-copper-oxide (BSCCO) being an example of HTS [11].

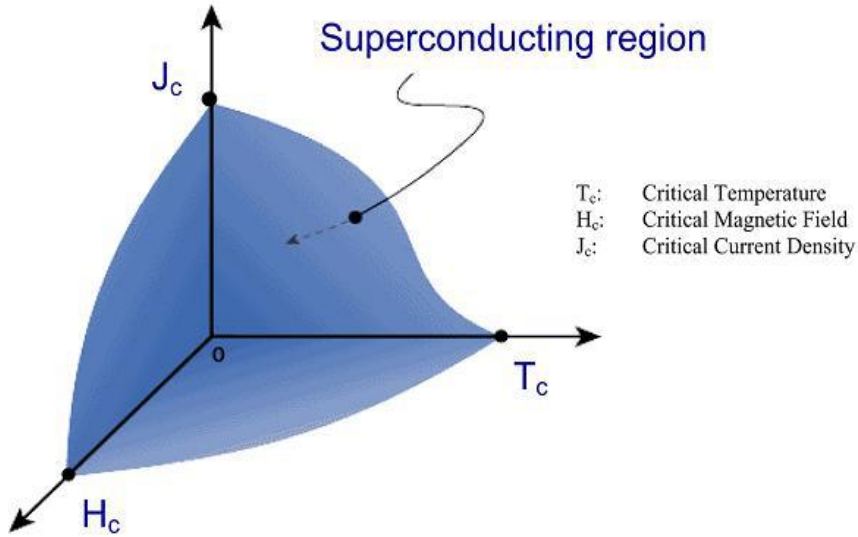


Figure 1: Superconducting region bounded by critical current, critical magnetic field, and critical temperature [16]

A material could only be classified as a superconductor when it is well-bounded in a superconducting region comprising temperature, current, and magnetic field. Figure 1 above illustrates the superconducting region of a material, and also portrays the interdependency of the boundary parameters of critical current density (J_c), critical magnetic field (H_c), and critical temperature (T_c). Critical current (I_c) will be referenced when discussing critical current density. The various parameters are briefly explained in the next section.

1.2.1 Critical Temperature

A superconducting material's critical temperature (T_c) is the specific temperature where the material transitions from an ordinary or resistive to a superconducting state. Hence, the material has no electrical resistance. However, the electrical resistance of superconducting material in its normal state or above T_c is higher than that of conventional or traditional conductors like aluminum and copper. A quench occurs when superconducting materials change from their superconducting state back to their resistive state.

From the classification of superconductors into LTS and HTS. LTS refers to a material having a T_c less than 30 K, while HTS refers to a material with a T_c greater than 30 K. MgB_2 , with a critical temperature of 39 K, has been classified as an LTS or HTS material [9], [15]. MgB_2 's composition is similar to that of other LTS materials, but its very high transition temperature is more akin to that of HTS materials. Table 1 below summarizes some superconducting materials as well as their corresponding critical temperatures [11].

Table 1: Superconducting materials and their transition temperatures

Superconductor	Transition Temperature (K)	Year Discovered
Nb	9.5	1930
NbTi	10.3	1962

Nb₃Sn	18.3	1954
Nb₃Al	18.8	1966
MgB₂	39	2001
REBa₂Cu₃O₇	93	1987
Bi₂Sr₂Ca₁Cu₂O₈	85	1993
Bi₂Sr₂Ca₂Cu₃O₁₀	108-110	1988

HTS materials exhibit better thermal characteristics as compared to LTS materials. As the operating temperature increases, the efficiency of a cryogenic refrigeration system also increases. The Carnot Coefficient of Performance is used to calculate the efficiency of cryogenic refrigeration systems and it is represented in the formula below.

$$COP_{cooling} = \frac{Q_c}{W_{in}} = \frac{T_c}{(T_H - T_c)} \quad (1)$$

Here, Q_c is the heat energy extracted from the cryogenic environment at the temperature T_c to maintain its cold state and W_{in} is the work-energy used for the refrigeration at the temperature to expel the waste heat. The improved thermal stability of HTS over LTS allows HTS to be utilized for power applications as the complexities and cost of the cryogenic infrastructure are significantly reduced.

1.2.2 Critical Current

When developing a superconducting device, one of the most significant parameters to take into consideration is the critical current of the superconducting material. This is because, there is a significant reduction in the overall space and weight due to the ability in utilizing the high current density that superconducting technologies possess over conventional technology. To make a superconducting device a viable replacement for conventional devices, the current density must be substantially higher in order to successfully balance the extra expenses of the superconducting device and necessary cryogenic refrigeration equipment[17]. According to research conducted in [18], replacing conventional copper cables with HTS cables resulted in up to 90 percent weight reduction. Ampere's law, as illustrated in the equation, may be used to calculate the critical current of an HTS cable.

$$\mu_0 J = \frac{dB}{dx} \quad (2)$$

From the formula, the permeability of free space is represented by μ_0 and it is 1.27×10^{-6} H/m. J depicts the locally averaged current density, B represents the locally averaged magnetic induction field, and is the measure of position.

Figure 2, a clear fast transition from superconducting to ordinary or resistive state can be observed. The related (I^2R) Joule heating will bring a considerable heat load into the system, with the potential to destroy the superconducting device, hence precaution must be taken to ensure that superconducting devices operate below the critical current as shown. A power law can be used to describe the transition from superconducting to the resistive state.

$$E_{Sc}(T) = E_c \left(\frac{I_{OP}}{I_c(T)} \right)^n \quad (3)$$

Here, n is the transition index variable, T denotes the absolute temperature and E_c denotes the electrical field that determines the critical current.

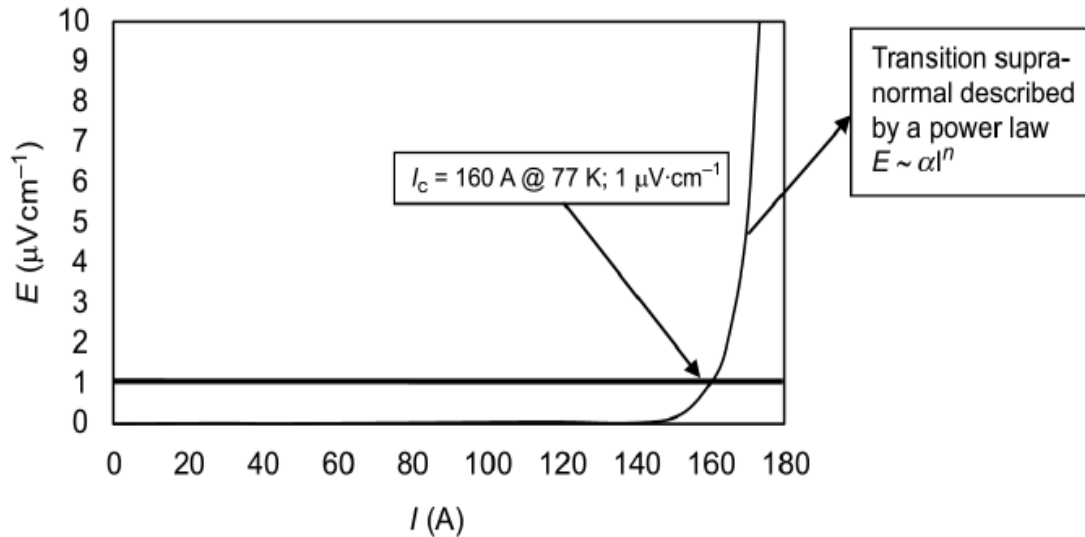


Figure 2: A graphical representation of a voltage-current dependency of a superconducting material [16]

From the superconducting boundary region in Figure 1 above, the interdependency of the critical parameters of critical temperature, critical current, and critical magnetic field can clearly be seen. An increase or decrease in any of the parameters, such as the operating temperature or magnetic field would have a resultant effect on the critical current of the material. Superconducting power applications that are fundamentally related by a substantial magnetic field like generators and motors, must have a lower operating temperature range of about 30 – 50 K to achieve the same critical current of a cable (60-80 K) which only has self-field. The operating temperature will reduce for a fixed magnetic field if the critical current of the superconducting material increases. The relationship between the HTS materials and the operating temperature for a fixed magnetic field represents one of linearity. However, for the LTS, the relationship under the same conditions is that of a curve. The critical current of an HTS cable, as an illustration, doubles when the temperature drops by 10 K, and the increase is proportional to the temperature drop. Figure 3 below shows the linear relationship between critical current and operating temperature for HTS materials.

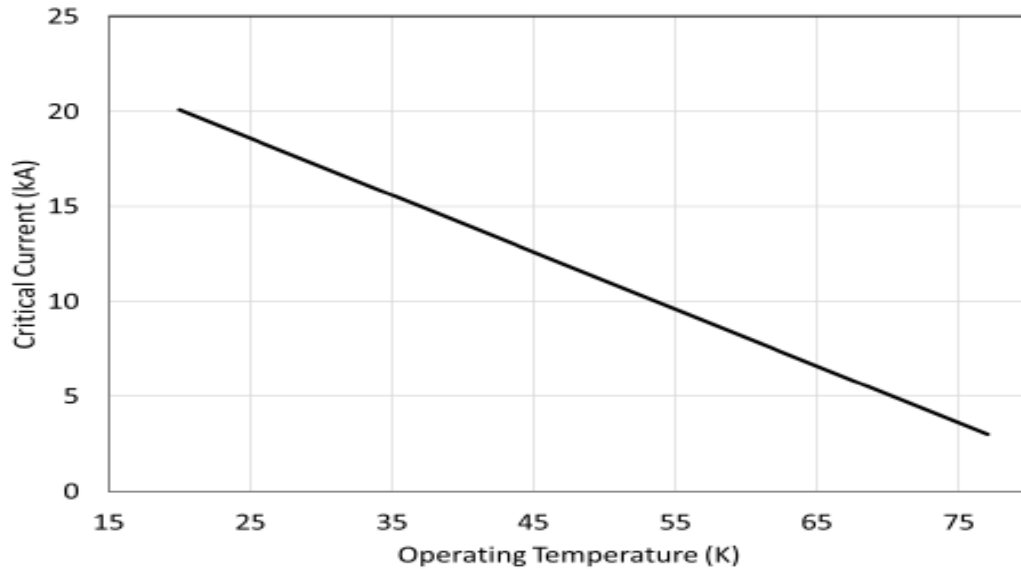


Figure 3: Linear relationship between critical current and operating temperature of HTS cable [19]

1.2.3 Critical Magnetic Field

Type I superconducting material was earlier described as materials that lose their superconducting properties in the presence of weak magnetic fields, for this reason, they are also known as soft superconductors. Also, Type II superconducting materials were defined as a type of material that could withstand strong magnetic fields before losing its superconducting property and could also be known as hard superconductors. Hence, soft superconductors have lower critical magnetic fields as compared to hard superconductors which have higher critical magnetic fields. Under specific circumstances (Meissner effect), both different types of superconductors become ideal diamagnets [16]. When a material becomes superconducting in a magnetic field, magnetic flux is ejected or expelled. The flux cannot permeate the material if a magnetic field is supplied after it has become superconducting. Except for a very thin layer on the surface, the Meissner effect allows the material to exhibit complete diamagnetism and prevents magnetic flux lines from penetrating the substance. This Meissner effect phenomenon is demonstrated in Figure 4 below.

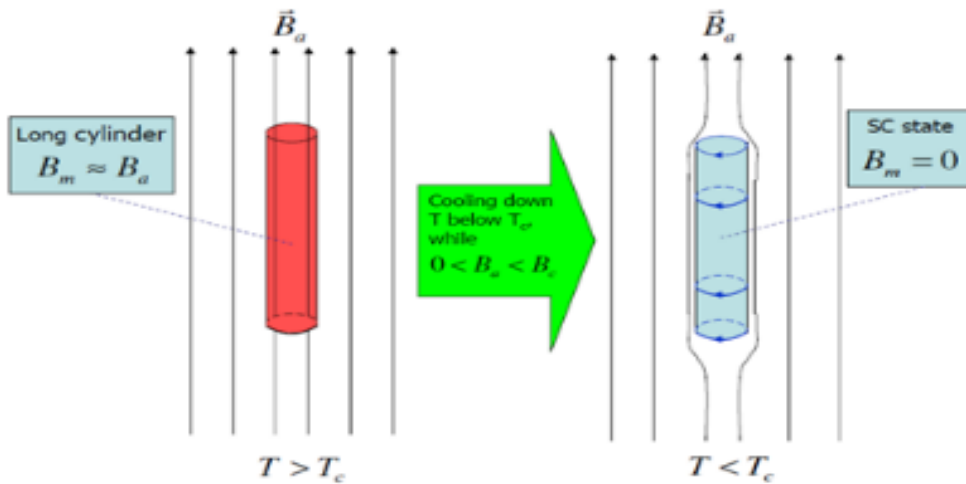


Figure 4: Meissner effect demonstrated by superconducting materials operating below both their critical magnetic field and temperature [16]

In some electric power applications, anisotropy is seen in the critical current of materials, and this can be problematic. The significant anisotropy in the superconducting properties of HTS materials is one of their most distinguishing properties. In contrast to isotropy, anisotropy is a feature of a material that permits it to alter or assume distinct characteristics in various directions. The effect of anisotropy cannot be overlooked and for that reason, critical current must now be reported as a function of applied magnetic field direction relative to the crystallographic axis, rather than only as a function of temperature and the magnetic field. HTS materials exhibit the highest level of anisotropy. Figure 5 and Figure 6 depict the critical currents of a REBCO-coated conductor versus the applied magnetic field at various temperatures, with the magnetic field parallel to the ab-plane and parallel to the c-axis.

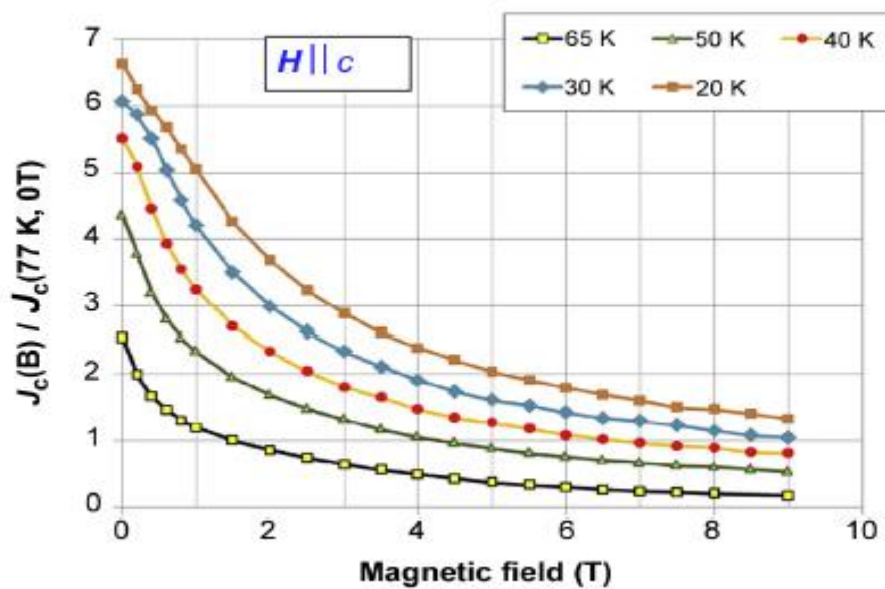


Figure 5: A graphical representation of J_c versus H along the c -axis at different temperatures for REBCO-coated conductor tapes [16].

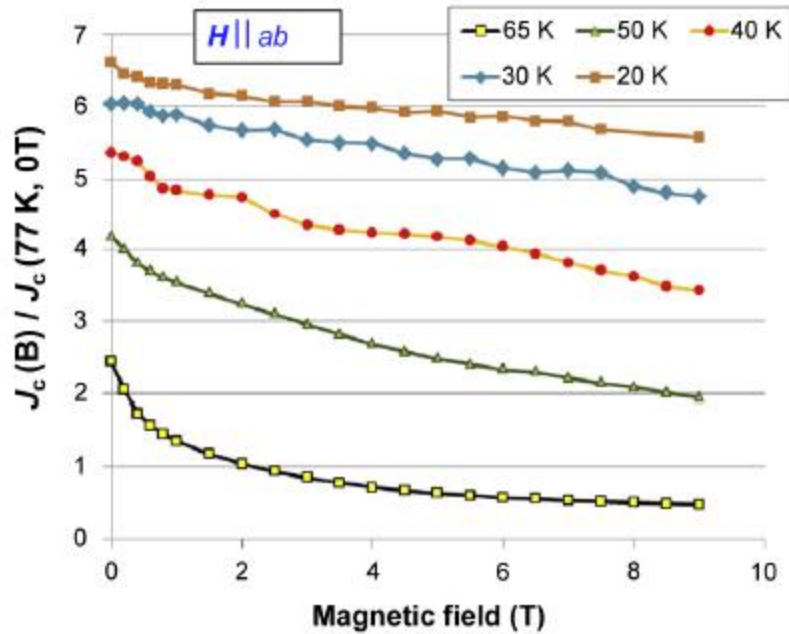


Figure 6: A graphical representation of J_C versus H along the ab plane at different temperatures for REBCO-coated conductor tapes [16].

The two graphs demonstrate the huge variation in J_C dependent on the applied field direction. The least J_C defines the highest current that a power application device like a generator, motor, or transformer can carry because magnetic fields affect a whole range of angles to the ab -planes of the superconducting tape. The lower J_C generated by the anisotropy has a detrimental impact on the device's size, mass, and cost since the lower J_C necessitates more turns in a magnet to produce the same number of ampere-turns.

2. Scientific question

The goal of the research is to fully understand the impact of electrical parallel faults on high-temperature superconducting (HTS) power cables used for medium voltage direct current (MVDC) shipboard power systems (SPS) of all-electric ships. The introduction of all-electric ships will produce a change in the processes of electric energy generation, transmission, and utilization. The desire for the ongoing research and advancement of all-electric ships by researchers including the Office of Naval research is sparked by the rising power demand of current navy ships as well as increased focus on the conservation of energy and environmental preservation. High-temperature superconducting (HTS) cables have high power density and power capacity and have been demonstrated to be advantageous for electric transport applications where space and weight are key design parameters. To achieve the ambitious power demands required by the all-electric ships and its power system, conventional copper cables will need to be replaced with HTS cables.

Generally, in the design of power systems, one of the difficulties is putting in safety measures to protect the system from potential electrical faults. Also, the failure of a component or a section within the system should not result in the total loss of the whole power system. In the case of SPS, it is vulnerable to abrupt changes in load due to the ship's mode of operation. Furthermore, because the components of the SPS are tightly connected and the systems are ungrounded, the SPS is more prone to electrical disturbances than a conventional terrestrial power system [20]. Hence faults that occur in an SPS system propagate to the entire system quicker than in long-distance terrestrial systems. If proper and adequate protection schemes are not incorporated, even minor fault scenarios might trigger catastrophic system failure in a densely coupled system. This is because, an electrical fault on an HTS cable technology could lead to damage of the HTS cable itself, vacuum failure, over-pressurization, and damage to the cryogenic infrastructure. The potential failure of HTS cables in SPS caused by an electrical fault and its consequences should be considered in the design process and in an event of a fault, it should not lead to other critical challenges to the cryogenic environment.

The reason for the interest in this research project is the impact that the findings or results will have in aiding in the development of fault tolerant HTS cable technology and design to mitigate the effects seen on the infrastructure when a pole-ground fault occurs.

3. High-Temperature Superconducting (HTS) power cables for electric transport applications

High-temperature superconducting (HTS) power cables have been developed, tested, and installed in electric power systems in several countries around the world [21]–[25]. Nevertheless, the HTS cable electrical or dielectric insulation designs are limited and several research projects are ongoing [26]. Maintaining the HTS power cables at their cryogenic operating temperatures to avoid heat leaks from ambient enabling it to achieve its high-power density and other benefits is another one of the major challenges currently being experienced. The cryostat is used for the circulation of the cryogen used to cool the cables. The HTS cables are housed by vacuum-jacketed cryostats which are able to provide thermal insulation and maintain a low-temperature gradient between the cryogenic temperature and room temperature. There are two dielectric insulation designs employed for HTS power cable insulations – warm and cold dielectric insulations. The cold dielectric insulation is where the electrical insulation is directly applied on the HTS cable and is in the cryogenic environment inside the cable cryostat. Several ongoing research is being conducted on the use and application of cold dielectric termination with the mismatch in coefficient of thermal expansion between the HTS conductor and polymeric insulation being a major challenge[27]–[29]. With the warm dielectric insulation, the electrical insulation used has no direct contact with the HTS cable and it is on the exterior of the cable cryostat, hence, the insulation is at room temperature [30]. This allows for traditional techniques of applying electrical insulation such as extrusion to be utilized. The warm dielectric insulation cables have been typically used for retrofitting works [31]. A single cryostat is used for the cold dielectric design, and this allows for higher power densities to be achieved as compared to the warm dielectric design which needs an individual cable cryostat for each cable phase. This makes the cold dielectric designs to be preferred as it contributes to the appreciable reduction in weight, space and cost of a system. In comparison with conventional cables, the power density of the HTS power cable for the warm dielectric insulation design increase by a factor of 3, and that for the cold dielectric insulation design increases by a factor of 5 [32]. Figure 7 shows the cold and warm dielectric insulation cable designs.

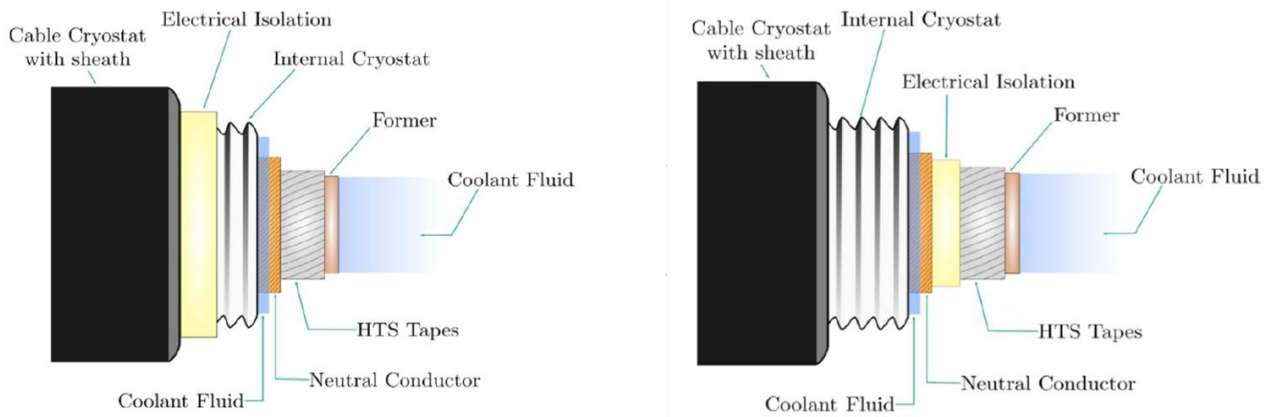


Figure 7: A warm dielectric insulation (left) and cold dielectric insulation (right) designs [33]

3.1 HTS Cable Designs

There are several acceptable three-phase HTS AC cable designs, but these are grouped into three. Namely, single core design, 3-core or triad design and HTS Triax™ design. The single core design is basically

made of a single-phase conductor placed in three individual cryostats. The main drawback of this type of design is the added weight of the three separate cryostats and the increase in the cryogenic cooling system needed. The 3-core or triad design utilize only one cryostat for all the three phases. The arrangement of the phases in the cryostat are done in a way to insulate each of the individual phases from each other and from the cryostat. In an event of a fault in any of the phases, the faulty phase can be replaced without affecting the other healthy phases. With this design, there is a reduction in weight and the overall cryogenic cooling needed. The Triax™ design is a trademark of Southwire Company. This type of HTS AC cable is designed to have three concentric phases contained in a singular cryostat. This ensures that the least amount of HTS tape is utilized and has the lowest impedance.

3.2 Choice of Cryogen

In designing HTS power cables, the choice of cryogen is an important parameter to be considered. The application of the HTS power cable should aid in the determination of the choice of cryogen used. This is because the choice of the cryogen will have a significant impact on the performance and cost of the HTS cable. HTS critical current density is temperature-dependent and it improves considerably at lower temperatures [9]. The capability of HTS cables to withstand high current densities makes it possible for medium voltage cables to be developed with high power ratings operating at lower temperatures.

The two most commonly used cryogens for HTS cables are liquid nitrogen and helium gas. Both have their own unique advantages and disadvantages. Liquid nitrogen (LN2) is the most utilized cryogen in the power grid or terrestrial HTS applications due to its ready availability and inexpensiveness, being non-flammable, having good heat capacity, and possessing excellent dielectric breakdown strength [34], [35]. LN2 poses some safety challenges where there is a risk of asphyxiation in confined spaces when there is a leak [36], [37] The safety concern coupled with the added weight makes using LN2 for HTS cables for electric ships applications not ideal.

Gaseous helium (GHe) is being investigated as a viable cryogen as it mitigates the challenges of LN2 and also has a larger operating temperature window, allowing for much higher power densities for various electric transport applications. Due to its low dielectric breakdown strength, GHe has only been a feasible alternative for medium voltage applications only. In a uniform electric field, the dielectric breakdown strength of GHe at 77K at 1.0 MPa is 4 kV/mm [38].

3.3 Cooling Cycles

Another important parameter to be considered in the design of an HTS system is the type of cooling cycle to be implemented. Generally, in maintaining the operating temperature for an HTS device, open-loop or closed-loop cooling systems are employed.

In an open-loop cooling system, the cryogen must be routinely replaced since it cannot be reused as a result of the cryogen boiling off. Open-loop cooling systems are conventionally implored because they are straightforward, affordable, and do not need the installation of cryocoolers. In operating open-loop cooling systems, liquid nitrogen (LN2) is typically used as the cryogen. This is because it is economical for a terrestrial system adjacent to the cryogen's production facilities [39]. For islanded power systems, such as electric aircraft and ship, it is not practical to implement an open loop cooling system. Nevertheless, research is being done to better understand the possibility of employing liquid hydrogen (LH2) as a fuel source for electric aircraft as well as a cryogen.

On the other hand, for the closed-loop cooling system, a cryocooler is installed as part of the HTS cooling system. The cryocooler removes waste heat from the cryogen that is fed back into the cryocooler and discharges it into a high temperature sink. The design of the closed-loop cooling system is complex and

costly. However, they are perfect for a shipboard system since they have a long time between maintenance cycles [39].

3.4 Cable Cryostat

HTS cables used in electrical power systems and other applications requires its temperature to be kept constantly low using a cryogen to be able to benefit from its superconducting properties. The flow of the cryogen to cool the cables is done inside a cryogenic envelope known as cable cryostats. The cryostat is designed to have a thin wall thickness to reduce the heat load that might be generated. Also, it is intended to achieve the smallest heat leak that is technically and economically viable. The technology has been fully optimized with a heat leak of around 1 W/mm into the cryogenic environment.

High thermal insulation along the cable is a major design requirement due to the potential to generate a considerable amount of heat load in a long DC cable system. Figure 8 shows a vacuum jacketed cryostat by Nexans.

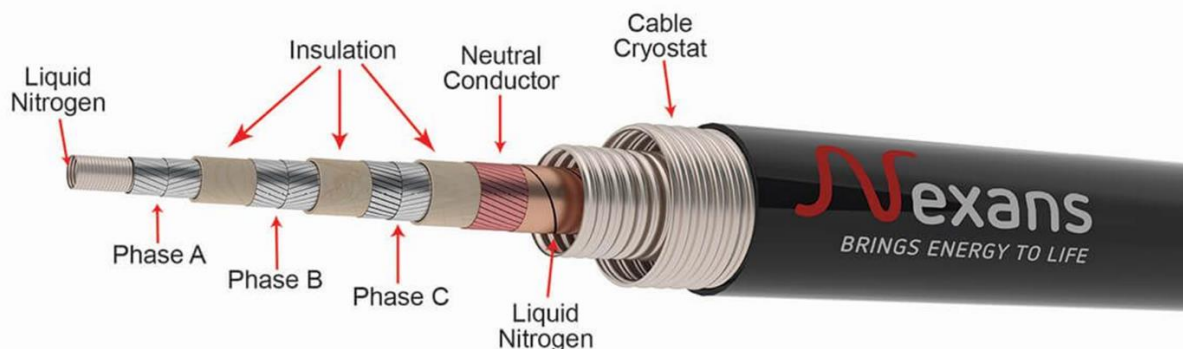


Figure 8 A vacuum jacketed cryostat by Nexans

3.5 Lapped Tape Insulation

Liquid nitrogen cooled and gaseous helium-cooled HTS power cables are generally insulated using a lapped tape insulation design. This is because only a small number of solid insulation techniques are applicable at cryogenic temperatures of 77 K for liquid nitrogen and below. The solid insulation generally cracks or breaks due to the mechanical stress it experiences under such cold temperatures and leads to insulation failure. Due to the significant temperature difference between room and cryogenic temperatures, there is a discrepancy in the coefficient of thermal expansion (CTE), and this results in mechanical stresses being experienced by the cable and its applied insulation. For this reason, cross-linked polyethylene (XLPE) is not a preferred choice of insulation for HTS power cables. Polyimide film insulations like polypropylene laminated paper (PPLP) and Kapton tapes are suitable candidates for HTS power cable insulation [30]. The polyimide film insulation which is manufactured in a tape form is helically wrapped around the length of the cable and allows for butt gaps to be introduced. The butt gaps are present to help alleviate the mechanical stress in the form of contraction shrinkage that the cables experience at cryogenic temperatures. The butt gaps also make it possible for the cables to be bent and coiled [30]. Figure 9 shows lapped tape insulation with butt gaps.

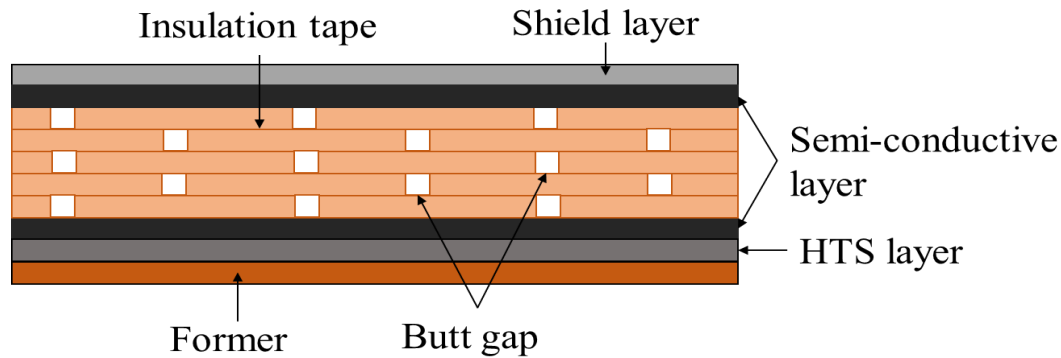


Figure 9: A lapped tap winding of HTS power cables with butt gaps showing the cross-sectional view [12]

The disadvantage of using lapped tape insulation with butt gaps is that it results in partial discharge (PD). The existence of PD activity has a direct impact on the electrical insulation of the HTS power cables, leads to the degradation of the insulation, and results in the failure of the cable [40]. The introduction of the butt gaps traps the liquid nitrogen (LN₂) and gaseous helium (GHe) used as the cryogenic coolant for the HTS power cables. For a GHe-cooled cable, the electric field enhancement caused by the dissimilarity in relative permittivity of the insulation tape and the GHe, in addition to the low dielectric strength of the GHe, causes PD to occur at the butt gaps with the trapped GHe. The voltage at which PD activity is generally detected for GHe filled butt gaps is lower than the actual dielectric withstand voltage of the cable. Partial discharge inception voltage (PDIV) is the minimum voltage at which PD is detected and as a result, it is critical to keep the HTS power cables below the PDIV to ensure the long-term performance of the cable. Due to the low voltage at which PD is detected for GHe-cooled HTS power cables with lapped tape insulation, the operation of the cable in applications is normally restricted to below 5 kV [41]. To address this significantly low operating voltage, numerous gas mixtures have been characterized and shown to enhance the dielectric strength when compared to pure helium gas [42], [43].

In an attempt to have a safe and improved dielectric strength of cryogenics for HTS cables, researchers have explored several gas mixtures by combining gases like nitrogen (N₂), Neon (Ne), and hydrogen (H₂) with higher dielectric properties to GHe [44]. Binary combinations of the gases were created, and AC breakdown measurements were performed at 77 K and compared to its pure and undiluted forms as shown in Figure 10.

From Figure 10, the same dielectric characteristics of the gas mixture of 4 mol% neon and 96 mol% helium were observed for pure helium. This result is coherent to the fact that when a small percentage of a gas medium of lesser dielectric property is combined with that of a stronger dielectric property, there is no appreciable change to the AC breakdown strength. The 4 mol% hydrogen and 96 mol% helium recorded the highest withstand voltage amongst the mixtures. The AC breakdown strength increases when a little amount of a stronger dielectric gas is combined with a weaker dielectric gas. Additional experiments and research are being carried out to look into different helium-to-hydrogen mixing ratios and their thermal properties associated. Park et al investigated and have provided additional information on the dielectric strength of He-based binary and ternary gas mixtures under cryogenic conditions while avoiding gas mixture condensation [45].

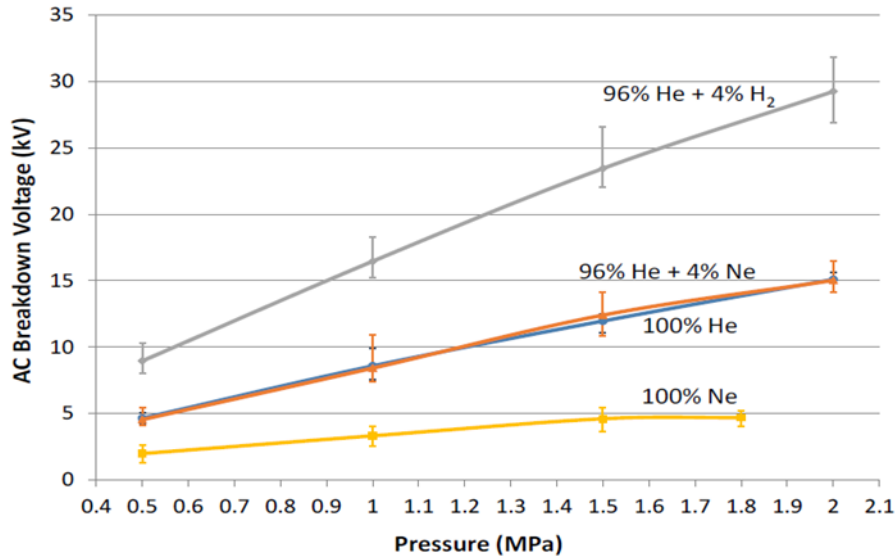


Figure 10 AC breakdown measurements for gas mixtures at different pressure levels for a 2-mm gap distance

New cable designs have also been developed to increase the dielectric properties of HTS power cables by utilizing the improved dielectric properties of helium-based gas mixtures.

3.6 Superconducting Gas-Insulated Transmission line

A new HTS power cable design has been fabricated to help solve the challenges that solid dielectric insulation (lapped tape) imposes in a cable setup. This gas-cooled and gas-insulated HTS cable design is termed as superconducting gas-insulated transmission line (S-GIL) and it is designed to use a cryogenic gas medium as both the dielectric medium of the HTS cable and the cryogen to cool the cable [46]. The lack of solid insulation in this setup precludes local electric field enhancements leading to higher operating voltages as compared to lapped tape insulation cables, and also with low partial discharge inception voltages. In [47], a GHe-cooled HTS power cable with the S-GIL design was developed and tested with 40 kV recorded as the maximum withstand voltage. This makes the S-GIL design ideal for a variety of electric transport applications including all-electric aircraft and ships. The voltage rating of the HTS power cable in this design is dependent on the pressure and the cryogenic operating temperature of the cable since the gas is used as both the dielectric medium and the cryogen. For this reason, it is critical to maintain the operating temperature and prevent any heat leaks into the environment. An advantage of this design is that, it eliminates any concern of internal partial discharge activity or discrepancy in the coefficient of thermal expansion resulting in dielectric insulation failure and also possesses better heat transfer capabilities.

In the design of the SGIL, insulation spaces are introduced in the cable setup to help isolate the cryostat from the HTS cable. These spacer materials employed have different relative permittivity to the cryogenic gas medium and hence cause electric field enhancement. This electric field enhancement created leads to surface flashover across the insulation spacers. This is a drawback associated with the SGIL cable design.

From the research and development of SGILs, the withstand voltage of the cable is influenced by two key parameters; the dielectric strength of the gas medium and the electric field enhancement created [48]. The dielectric strength of the gas medium is dependent on the fixed density of the gas medium. Several experiments under different conditions have been conducted to study and understand the possible withstand voltage and high-voltage stresses for the SGIL design. A sample SGIL model cable experiment that had

helical spacers installed to isolate the cable from the cryostat and not inhibit the flow of the cryogen was conducted. Figure 11 below shows the withstand voltages of pure GHe and a gas mixture of 4 mol% H₂ and 96 mol% of GHe as a function of the pressure of the gas medium at 77 K. From the figure, the highest withstand voltages were recorded to be approximately 35 kV and 23 kV for the H₂-GHe gas mixture and pure GHe respectively.

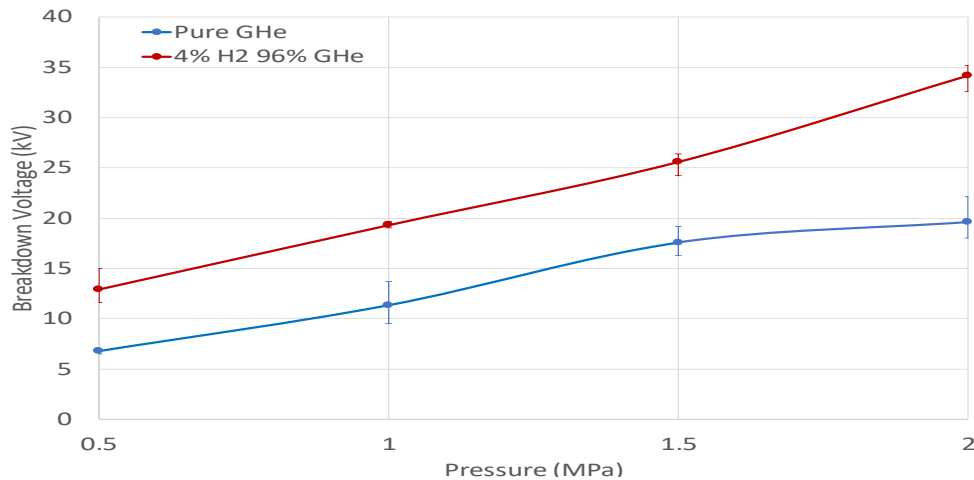


Figure 11 AC breakdown voltages of pure GHe and a gas mixture of 4 mol% H₂ and 96 mol% of GHe as a function of pressure at 77 K

These results were significantly lower as compared to earlier experiments conducted in [48] where the helical spacers were not used. The helical insulation spacers used created electric field enhancement and resulted in a surface flashover, leading to lower withstand voltages as recorded. A noticeable positive outcome of the spacers used at the cryogenic temperature was that the spacers didn't crack or break and were able to withstand the thermal shocks introduced from room temperature to 77 K.

To improve the voltage at which the surface flashover was occurring, research is ongoing in optimizing the design and material used for the spacer while taking into account the design of the space for optimum cryogen flow.

3.7 Power System Architecture of Electrical Ships

As earlier stated in the previous sections, HTS technologies are being developed for large electric transport applications, and to make this attainable and practical, power-dense devices and architectures are needed [49]. Since HTS applications operate at cryogenic temperatures, the cryogenic cooling system should be considered as a key parameter in the design of power systems for transport applications. The electrical and thermal properties of HTS applications specifically cables should also be taken into consideration in the design of the power system topology because the positioning or location of the cryogenic systems is dependent on that. Also, during the design process, redundancy systems should be incorporated in order to handle critical loads in an event of a fault.

To achieve high efficiency, high power density, resiliency, and robustness at the system level, [49] and [50] discussed the electrical and cryogenic systems of power system architecture for all-electric ships. A notional 4-zone radial power distribution system architecture was designed with a power rating of 100 MW. The individual electrical zones had non-uniform power ratings with the largest electrical loads located in zones 2 and 3. The fundamental advantage of having a radial architecture over a ring or dual bus architecture is

the ability to utilize the wide range of variable current ratings of HTS cables that is, able to have lower or higher ampacities. Also, the shorter distances between the generators and electrical loads make it a viable option to have a radial architecture. *Figure 12* depicts the architecture of the designed circulation system as discussed in [50] operating under normal conditions.

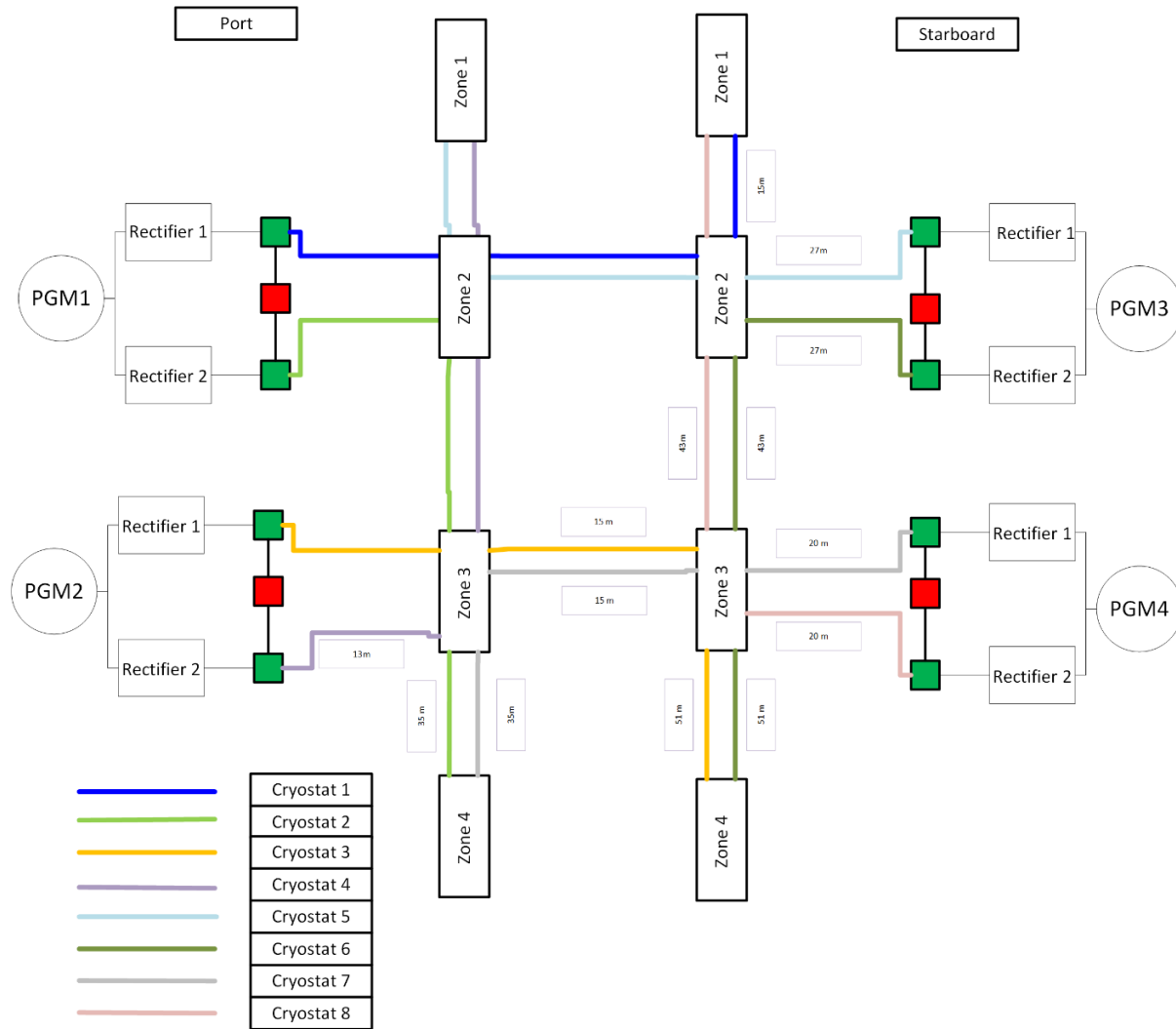


Figure 12 A schematic of a cryogenic circulation system operating under normal conditions [21].

To make the power system resilient in an event of a cryogen circulation failure by a cryocooler, zones 1 to 4 have additional cable routes, with several cryostats terminating at zones 2 and 3. This is to provide redundancy for the system. Also, to help prevent a total collapse of the network during a failed circulation at a particular section, the architecture is designed to divert or reroute the flow of the cryogen to the HTS devices to maintain the optimum cryogenic operating temperature. In [49], two notional radial cable architectures were studied where hybrid HTS and dipole cables were employed. *Figure 13* below demonstrates the radial cable architecture utilizing the hybrid cryogen HTS cable. The basis for this architecture is to reduce the heat load on the cryogenic system in order to achieve a high-power density solution that is both efficient and effective. In this design, the cable pathways are dependent on the three

terminating locations that are served by a single cryostat and also demonstrate the protection devices' switching state.

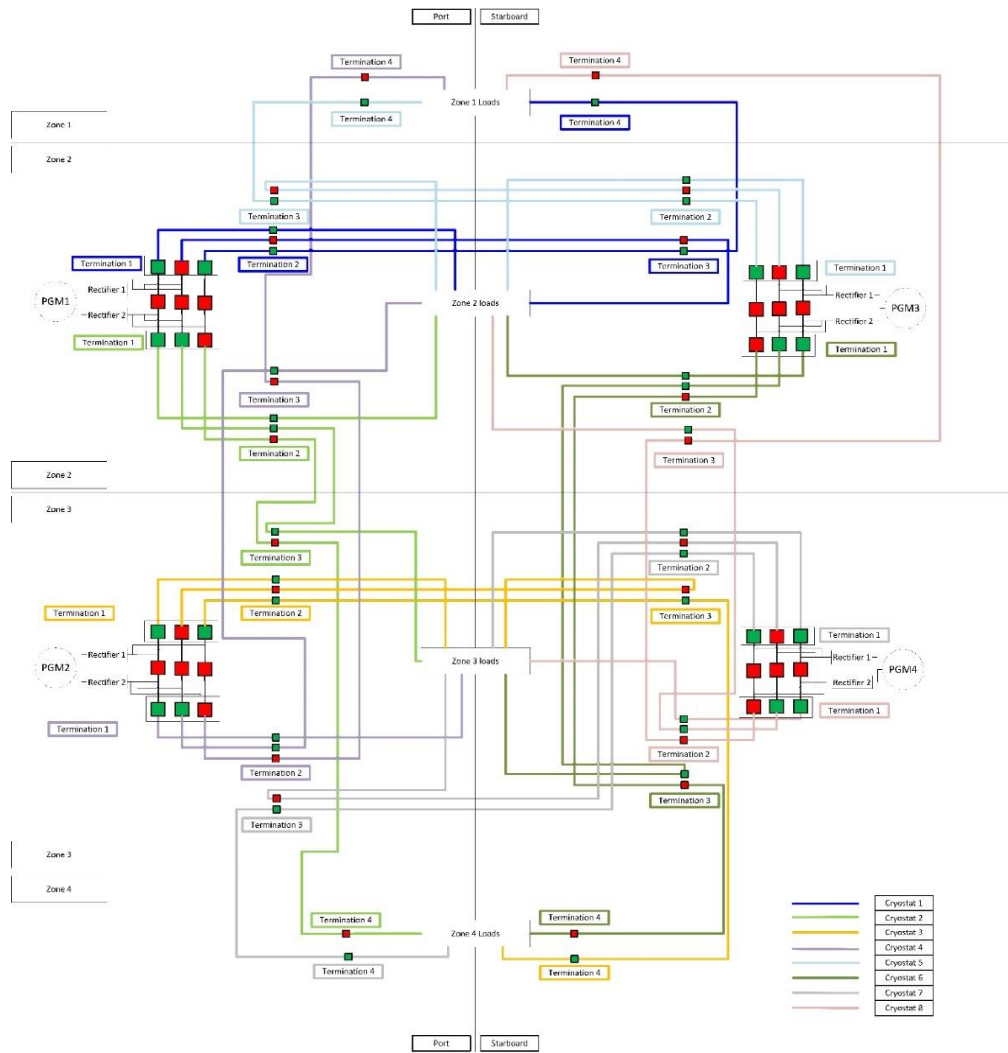


Figure 13 Radial cable architecture utilizing hybrid cryogen HTS cable [20]

4. Electrical Faults in HTS power cables of MVDC systems

When designing an HTS power cable for MVDC power systems, it is essential to consider the possible electrical fault scenarios that HTS cables must tolerate. An efficient and effective power system should be stable, resilient, and offers redundancy in the event of a fault. In a large electric transport system, failure of a component or a section of the system should not lead to the loss of the whole power system which in turn will be catastrophic. One of the major challenges in designing shipboard power systems (SPS) is putting in mitigating measures to protect the system from potential electrical faults and minimize the damage in case of a fault. the ship's operational mode, makes the SPS vulnerable to abrupt changes in load. Furthermore, the components of the SPS are tightly connected and the systems are ungrounded. Hence, the SPS is more prone to electrical disturbances than a conventional terrestrial power system. Because of this, faults that occur in an SPS system propagate to the entire system more quicker than in long-distance terrestrial systems. If adequate protection schemes are not incorporated into the system, even a minor fault might trigger fatal system failure. This is because, an electrical fault on an HTS cable could lead to damage to the HTS cable, vacuum failure, over-pressurization, and damage to the cryogenic infrastructure. The potential failure of HTS cables in SPS caused by an electrical fault and its consequences should be considered in the design process and in an event of a fault, it should not lead to other critical challenges to the cryogenic environment. The shipboard power system should be designed to handle these rapidly spreading fault circumstances and be capable of completely and swiftly returning to normal operation following an electrical fault scenario.

4.1 Types of DC electrical Faults

The electrical faults experience can be categorized into two groups: parallel and series faults [51]. A parallel fault occurs when there is an electrical connection between two wires or conductors of different voltages. A typical example in an MVDC is a pole-to-ground fault and a pole-to-pole fault. These types of faults are caused by insulation failures and cause a short circuit in the system. A plasma arc is created as a result of this. Once the plasma arc is created there is the potential for a pole-ground fault to propagate to a pole-pole-ground fault.

A series fault on the other hand refers to when an electrical connection exists between two or more points within the same phase. A high-impedance arc channel may be produced by a series fault which may originate from a partially detached conductor or disconnected cable. Due to the series design, the conductor's load current cannot be greater than the arc current. Series arcs typically don't provide enough heat energy to start a fire. Hence, the corresponding protection device in the power system may not be triggered at all. However, the effect of the plasma arc will cause a dielectric breakdown by the change in temperature inside the cable and may lead to challenges in the cryogenic environment.

Parallel faults are of great concern due to the fault current generated being significantly higher than the nominal current. A short circuit measurement can be used to estimate the magnitude of the fault current. In equation (4), the fault current introduced into a system is estimated by transforming the circuit into a Thevenin equivalent circuit. This allows for ease of calculation and accurate determination of the current.

$$I_{fault} = I_{SC} = \frac{V_{th}}{Z_{eq}} \quad (4)$$

4.2 Causes of parallel faults and their associated impact on power systems

As discussed earlier, a pole-to-pole and a pole-to-ground faults are the possible DC parallel faults that can exist in an HTS cable system. Also, there is the possibility of a pole-to-pole-ground fault occurring depending on the cable configuration. For the cable configuration, either a monopole or dipole configuration is anticipated. The magnitude of the fault current and energy released for the pole-to-pole-ground is much more catastrophic in the cryogenic environment than the other two types of faults[42]. Typically, a pole-to-ground fault could develop and become a pole-to-pole-ground in a dipole cable configuration and become devastating. These faults result in dielectric insulation breakdowns and cause a change in temperature which affects the overall cryogenic system. This change in temperature could result in a significant increase in the cooling power needed for the MVDC power system. Cable quenching is also experienced in the HTS power system in an event of a fault. An HTS tape quenches when it switches from a superconducting state to a resistive state. This means the critical current of the HTS tape has been passed. In the resistive state, its current carrying capability drastically reduces and if the fault current is not subdued, there is the possibility the HTS tape may sustain irreparable or permanent damage. Also, due to the intensity of the fault, the vacuum-jacketed cryostat can be punctured leading to a cryogen leak and thermal runaway.

4.3 Damage to the cryostat

For the HTS cable to maintain the right thermal insulation from ambient and the required cryogenic operating temperature, a cryostat is used. This makes the cryostat a crucial part of the HTS system. Cryostats that are currently in use have vacuum jackets that makes them expensive, and the corrugated walls that maintain the vacuum make them heavy. Hence, the cryostats are considerably heavier than the HTS cables. The cryostats are susceptible to failure in the event of a vacuum breach due to the requirement for a high vacuum, which is essential for thermal isolation. Consequently, the integrated cooling system needed to maintain the cryogenic temperature raises more questions about the cable system's potential for an electric failure. This is because the system is critically dependent on both electrical and thermal conditions rather than simply electrical conditions. Damage or puncture as a result of a fault to the cryostat is detrimental to the HTS power cable and the overall system as a whole. The next few sections describe the experimental setup and measurement procedure designed to investigate the level of fault current needed to puncture a stainless-steel cryostat.

5. Experimental Setup and Measurement Procedure

To understand the impact of electrical faults on HTS cables, a high current measurement is performed at two different temperatures. The first at room temperature of 300 K and at cryogenic temperature of 77 K using liquid nitrogen. The experimental setup was designed and interfaced with a high current unit to accommodate the two different temperature variations. The approach and design of a model HTS cable and its cryostat used throughout the different measurements were kept constant. The importance and use of the cryostat in the HTS cable arrangement is adequately described in section 3.3 above. A corrugated stainless steel tube of inner diameter of 39 mm, outer diameter of 44 mm and wall thickness 2.5 mm is used. It is cut into 154 mm and 334 mm lengths to house the model HTS cable. For the design of the model HTS cable, aluminum rods of 133 mm and 299 mm in lengths were cut uniformly. The longer length of the cable was to make it possible to accommodate the traveling of an arc as a result of a higher fault generated. To be able to create an electrical fault, there should be an electrical connection between the model HTS cable which is at potential, and the cryostat which is at ground potential to create a short circuit. A tracer wire of 0.35 mm in diameter is used as the electrical connection needed to create the short circuit. This wire is connected to the aluminum rod as twenty (20) layers of polypropylene laminated paper (PPLP) are wrapped as insulation around the rod. The cable is completed by wrapping a shield layer of copper tape of thickness 0.066 mm around it. The HTS cable and the cryostat are kept at the same potential using a ground wire. Furthermore, the HTS cable rest on the bottom of the cryostat which allows the shield layer to create an additional grounding path for the cable. A cut section and front view of the HTS model cable arrangement are shown in Figure 14 below.

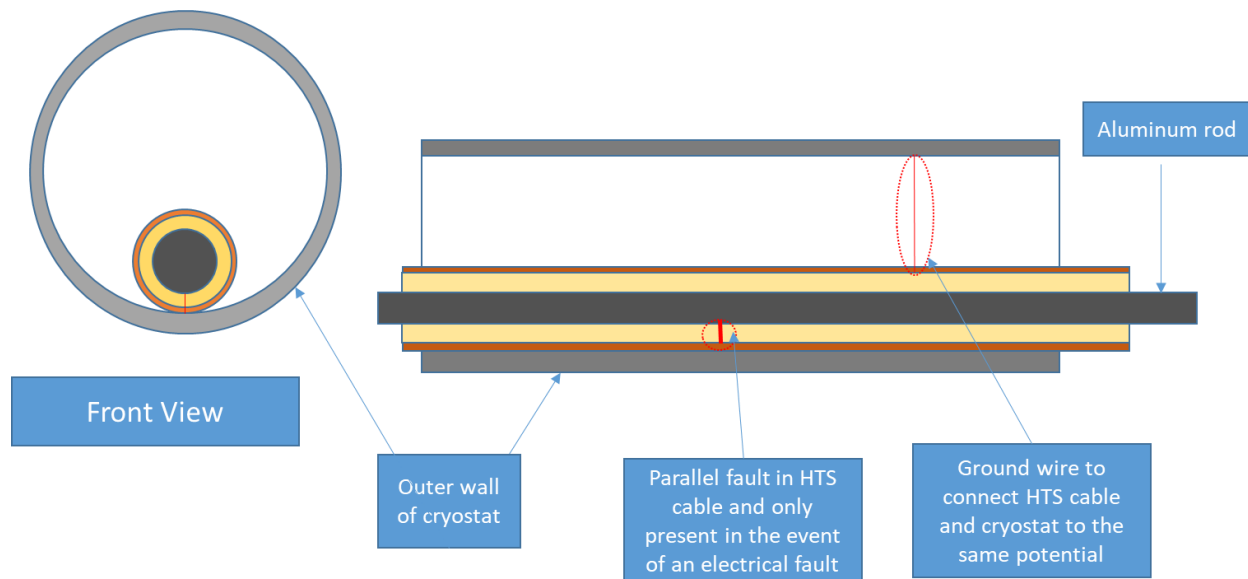


Figure 14 A cut section and front view of the HTS model cable arrangement

Figure 15 shows a high current circuit arrangement used to perform the high current measurements. The maximum charging voltage of the circuit is up to one (1) kilovolt (kV), with a current capacity of up to 100 kA. It has an adjustable resistance with a minimum value of 65 m Ω and can record a minimum

inductance of $10 \mu\text{H}$. Also, it has adjustable four capacitor towers that can be connected and produce capacitance in the range of 85.5 mF and 300 mF . The total capacitance for the system depends on how many capacitor towers are connected and triggered. Two differential probes of the type TT- SI 7005 with $1 \text{ M}\Omega$ input impedance (differential), 50 MHz bandwidth @ $\times 5$ attenuation setting, $\pm 18 \text{ V}$ (DC + AC peak) common mode and with a high accuracy of $\pm 2\%$ is used. The use of the probes in the experimental setup is to assist in the correct recording of the total capacitor voltage and the arc voltage that will be produced as a result of the fault current. A rogowski coil of type CWT MINI 150 with a peak current reading of up to 30 kA is used to measure the fault current that will be generated. A coaxial shunt resistance of $0.2547 \text{ m}\Omega$ is used together with a differential probe to also measure the fault current. This serves as a form of verification for the rogowski coil measurement reading.

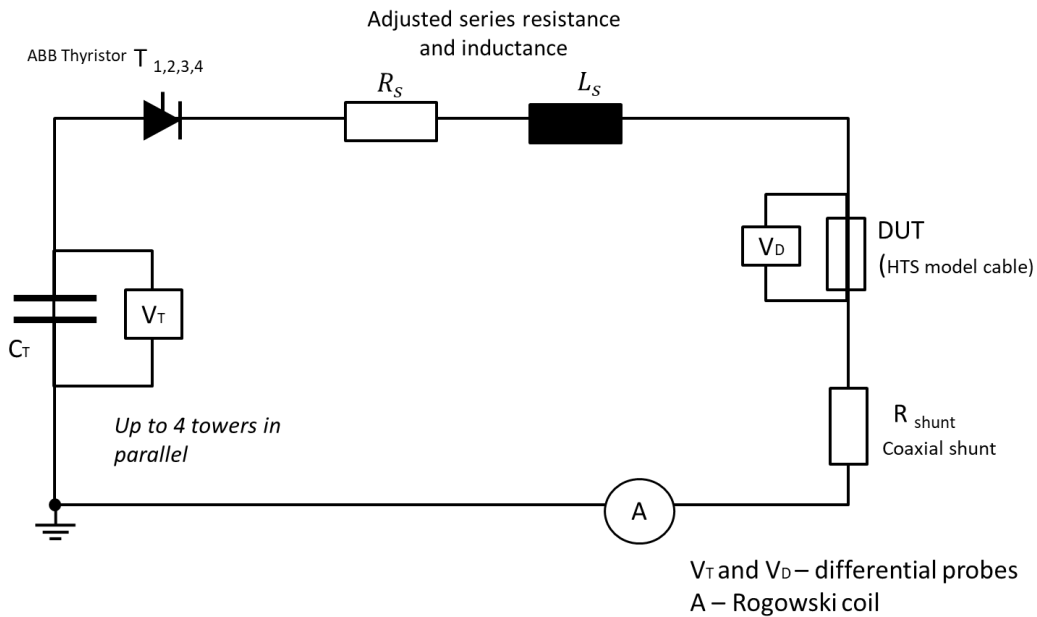


Figure 15 High current circuit arrangement

For the cryogenic temperature measurement, the setup for the device under test which is the HTS model cable slightly changes from that of the room temperature arrangement. The HTS cable is placed in an open bath of liquid nitrogen to be able to achieve the desired temperature of 77 K . The cable is vertically oriented in the liquid nitrogen bath to allow for the capturing of arc using an industrial high speed camera. The industrial high speed camera is included in the experimental setup to be able to film the measurements and have a better visual representation and understanding of the arc or fault produced. The high speed camera is a Photron FastCAM model SA-Z which has a colored video feature with 648×299 pixels at a framerate of $100,000 \text{ fps}$. Different camera settings are adjusted for both room temperature and liquid nitrogen measurements. Also due to the high light intensity that is produced as a result of the arc, different filter (stops) are installed on the camera to limit the light intensity that is captured. Table 2 shows the different camera settings used in the experiment.

The placement of the camera relative to the device under test is crucial in recording the measurements. For the liquid nitrogen open bath measurement, due to the vertical orientation of the cable, a mirror is utilized alongside the high speed camera. The mirror is positioned at an angle to be able to reflect the HTS cable in the liquid nitrogen bath. This also helps to keep the high speed camera at a distance to help safeguard it

from a spillage or splash of the nitrogen as a result of the measurements. Figure 16 shows the setup for the liquid nitrogen measurement.

Table 2 High speed camera settings for the various measurement requirements

Current Level (kV)	Shutter speed (sec)	Filter (Stops)	Insulation Medium
1	1/630000	3	Room temperature
5	1/266667	5	
8	1/266667	5	
10	1/400000	5	
1	1/630000	3	Liquid Nitrogen
5	1/630000	5	
10	1/400000	5	

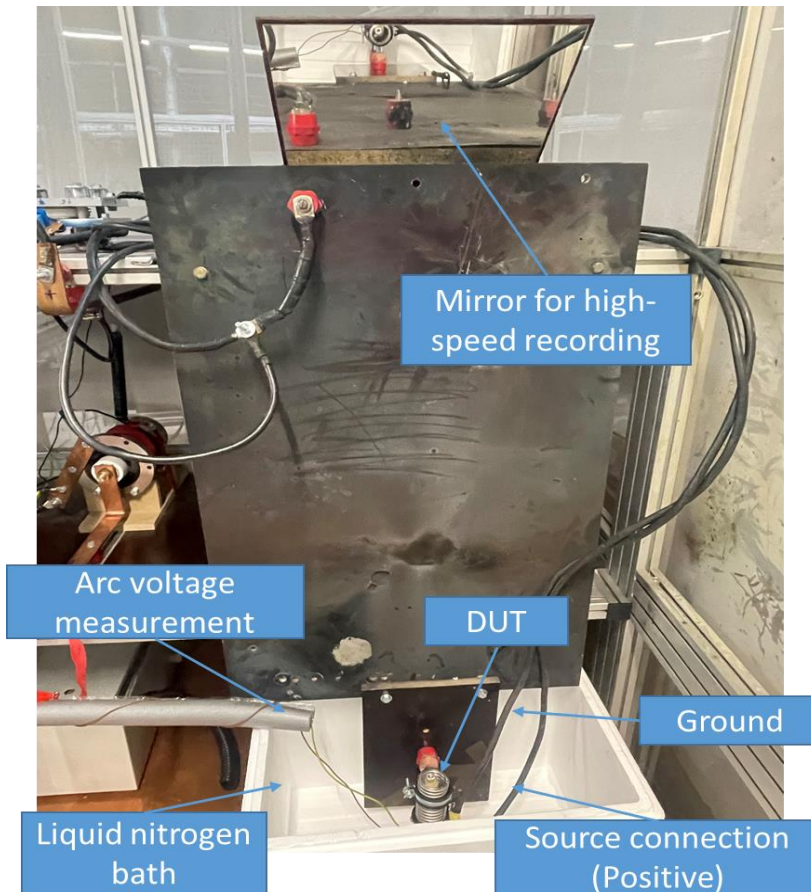


Figure 16 Setup for liquid nitrogen measurement

Experimental matrix was designed for both 300 K and 77 K measurements to understand the impact of the electrical faults on the HTS cable and cryostat. These measurements considered fault current measurements in the range from 1 -10 kA at a voltage level of 1 kV and with a capacitance of 330 mF. From the high current circuit arrangement discussed above, the resistance and inductance of the circuit were always configured and adjusted to achieve the required current level for each measurement. A short circuit experiment is performed before the actual measurement to calibrate and ensure;

- accurate reading of all the recording instruments in the circuit; the voltage probes, the rogowski coil, the oscilloscope and the high speed camera.
- the triggering of all four capacitor towers to achieve the required capacitance and voltage.
- the adjusted resistors produce the needed resistance and inductance to achieve the fault current rating.

The device under test is now connected as part of the circuit after the short circuit test, for the actual measurement to be carried out. The results are recorded, stored and analysis with the help of a matlab simulation tool.

6. Results and Discussion

The results of the measurements at room temperature and 77 K are presented in this section. All the waveform graphs and pictures of the device under test after the measurement are included in the appendix. All the experimental conditions were kept consistent and constant for the two temperature measurements. Figure 17 shows a typical waveform for the measurements. The recorded parameters include the arc voltage, arc current and the capacitor voltage. The capacitor voltage is the charging voltage of the circuit. The graph is plotted with two y-axis of voltage in volts (V), current in kilo amperes (kA) and an x-axis of time in milliseconds (ms).

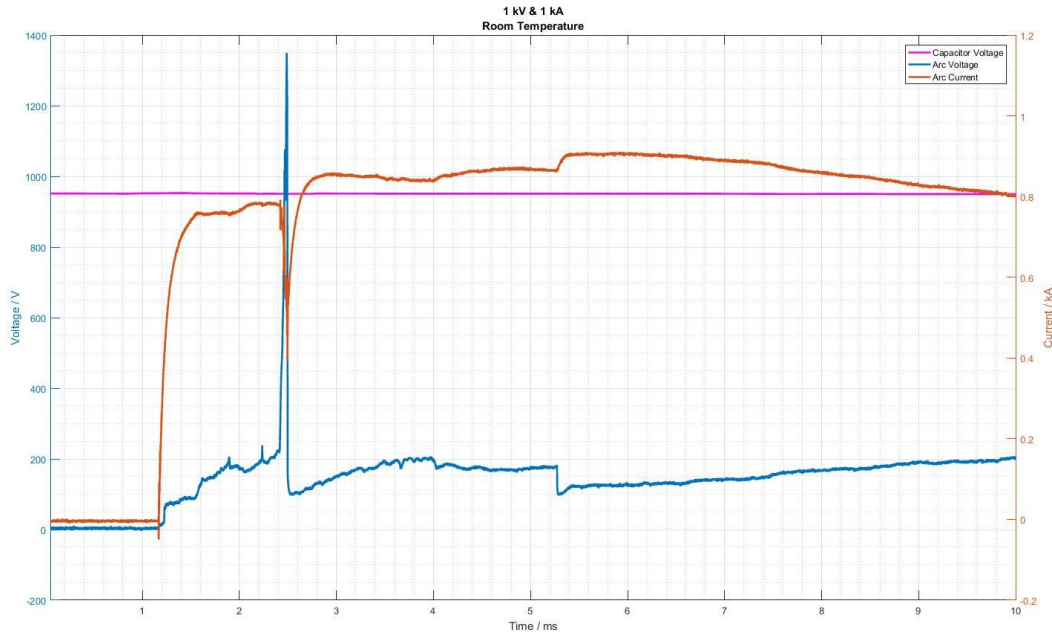


Figure 17 A typical waveform for the measurements

The arc was generated by creating a short circuit between the HTS model cable at potential and the stainless steel tube cryostat which is at ground potential. The tracer wire or “initiator” wire vaporizes and establishes a bridge of thermally ionized air which becomes a channel for the arc to travel in the tube.

For the room temperature measurements, a total of 4 different current level measurements were performed; 1 kA, 5 kA, 8 kA and 10 kA. The results of the experiments were subjected to visual examination afterwards. The 1 kA and 5 kA measurements had no perforations on the cryostats after the arc was extinguished. It was observed that at 2.4 ms, the arc voltage reached a peak of 1380 V for the 1 kA. At this peak, the arc was observed to have come out of the stainless steel tube. However, there was some discoloration along the inner wall of the tube as the arc traveled along the axis of the tube for the 5 kA. For the 8 kA and 10 kA measurements, perforations were observed on the stainless steel tube. These perforations made had different sizes for the different current levels. The 8 kA was recorded to have a 35 mm size hole and the 10 kA had 47 mm. These dimensions were measured across the longest axis of the hole, as the holes are not perfectly circular. Figure 18 and Figure 19 shows the waveform for 8 kA and 10 kA measurements.

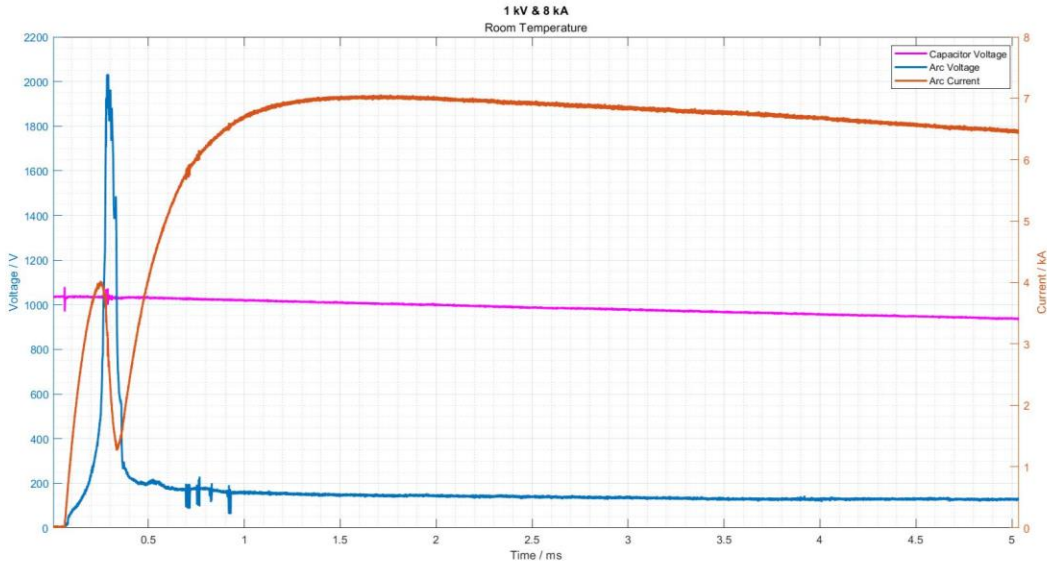


Figure 18 A waveform measurement for 8 kA at room temperature

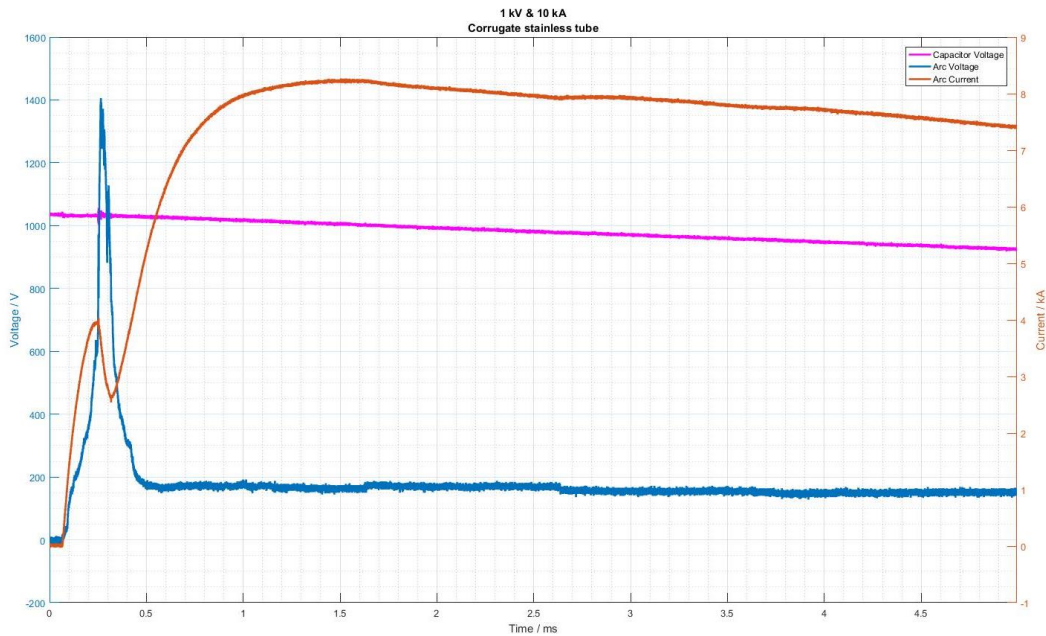


Figure 19 A waveform measurement for 10 kA at room temperature

For the liquid nitrogen measurements, a total of 3 different current levels were investigated; 1 kA, 5 kA and 10 kA. The arc produced at 1 kA did not cause any damage either within or outside of the cryostat tube after visually inspecting it. The arc extinguished after 5 ms. Perforations were observed for both the 5 kA and 10 kA measurements. It was observed that the arc took 1.4 ms for the 8 kA measurement and 0.4 ms for the 10 kA measurement to perforate the two tubes. Unlike the room temperature measurements, where one punctured hole was observed and could easily be measured. There were several holes along the axis of the tube observed for the liquid nitrogen measurement. The path of these holes signified the travel path of

the arc that was generated. The arc sustained at the ends of the tube, burning off the ends of the tube and the HTS model cable (conductor) till it finally extinguished. A closer examination of the conductors for both measurements showed a normal geometry of arc notch with a raised part at where the tracer /ignition wire was located. The notch depth was a slight surface indentation. The arc voltage for the 10 kA (3100 V) was twice that of the 5 kA. Figure 20 and Figure 21 shows the waveform for the 5 kA and 10 kA measurements.

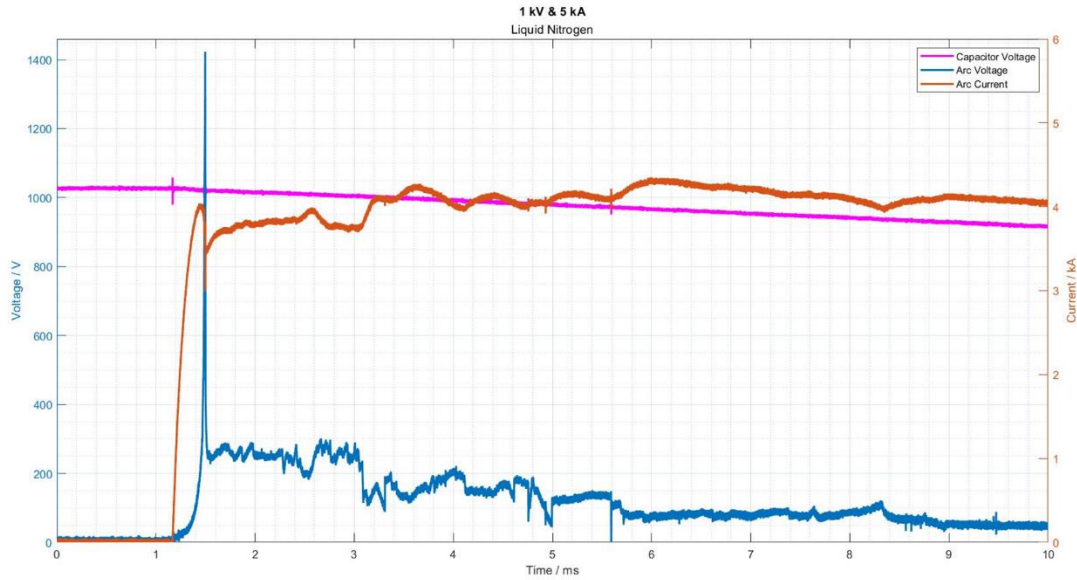


Figure 20 A waveform measurement for 5 kA at 77 K

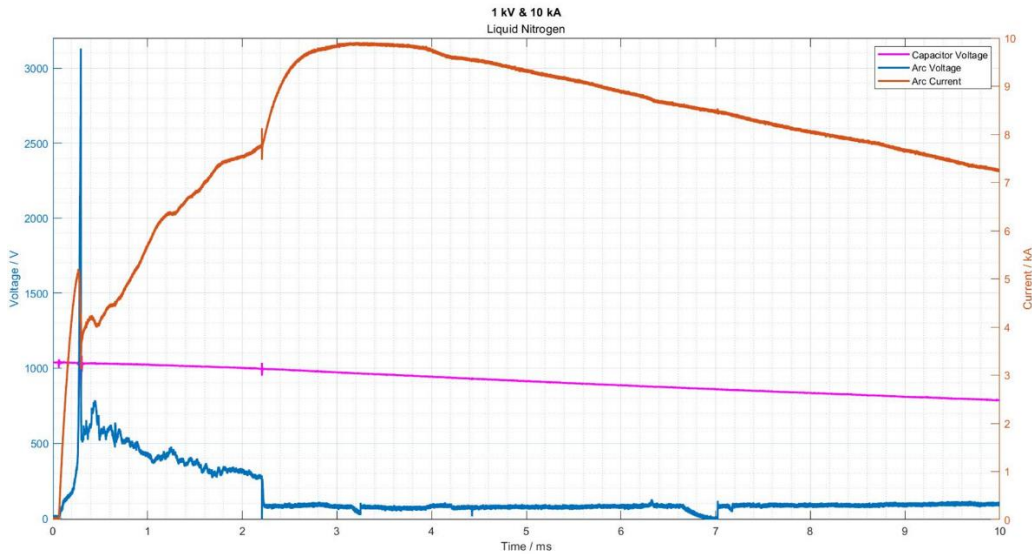


Figure 21 A waveform measurement for 10 kA at 77 K

7. Conclusion and Future Work

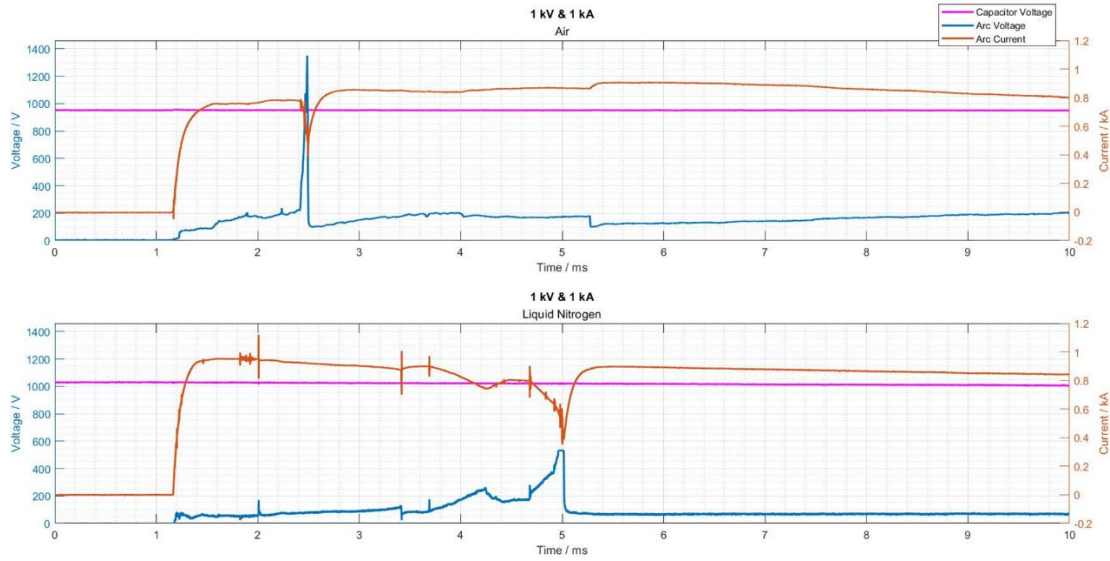
The estimated operating current for all electric ships is expected to be between 1 kA – 5 kA. Any electrical fault is expected to increase the operating current by a factor of 3 or 4. This implies that fault current is expected to reach 20 kA. With the results from the measurements, the operating current for the MVDC for the SPS will need to be reviewed. This is because damage to the cryostat by an electrical arc could lead to thermal runaway. Also, the damage could be detrimental to the overall power system. Where the damage to the cryostat may lead to a vacuum leak which in turn will lead to a substantial heat leak from the ambient. Depending on the installation of the cables in the power system, this leak if the cryogen is liquid nitrogen, could eventually lead to asphyxiation.

These results also provide guidance in improving HTS cable technology to be fault-tolerant, allowing them to recover from probable faults in the power system. The cable topology will need to be revised to protect the cryostat from damage. Future studies and experiments are needed to fully understand the arc physics that is generated in the tube. Also, it is imperative to understand the withstand strength of the cryostats after a fault. Hence a number of measurements will need to be performed on the same cryostat to understand the effect when a fault reignition occurs in the power system.

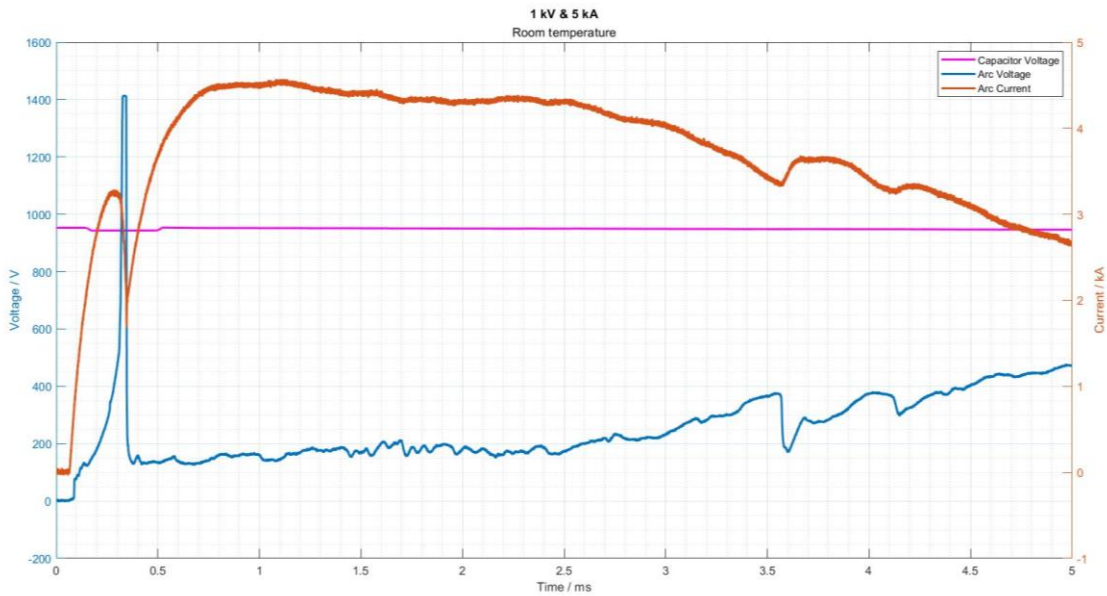
Based on the preliminary findings of this research, the experimental data collected will be potentially presented in two IEEE publications. Namely, IEEE transactions on applied superconductivity and IEEE transactions on dielectrics and electrical insulation journals. The publications will investigate fault propagation along the HTS cable. This is paramount to help with the protection of the other superconducting devices, the cryogenic environment, and also the overall power system architecture.

8. Appendix

Results for 1 kV & 1 kA both in RT and LN2



Results for 1 kV & 5 kA Room temperature





Cryostat for 10 kA RT measurements



Cable in stainless-steel tube for 10 kA RT measurements



Conductor and cryostat for 5 kA LN2 measurement



Conductor and cryostat for 10 kA LN2 measurement



Cryostat for 1 kA LN2 measurement

9. List of figures

Figure 1: Superconducting region bounded by critical current, critical magnetic field, and critical temperature [3]	6
Figure 2: A graphical representation of a voltage-current dependency of a superconducting material [3] ..	8
Figure 3: Linear relationship between critical current and operating temperature of HTS cable [7]	9
Figure 4: Meissner effect demonstrated by superconducting materials operating below both their critical magnetic field and temperature [8].....	10
Figure 5: A graphical representation of JC versus H along the c-axis at different temperatures for REBCO-coated conductor tapes.....	10
Figure 6: A graphical representation of JC versus H along the ab plane at different temperatures for REBCO-coated conductor tapes.....	11
Figure 7: A warm dielectric insulation (left) and cold dielectric insulation (right) designs [21].....	13
Figure 8 A vacuum jacketed cryostat by Nexans	15
Figure 9: A lapped tap winding of HTS power cables with butt gaps showing the cross-sectional view [28]	16
Figure 10 A cut section and front view of the HTS model cable arrangement	23
Figure 11 High current circuit arrangement.....	24
Figure 12 Setup for liquid nitrogen measurement.....	25
Figure 13 A typical waveform for the measurements	27
Figure 14 A waveform measurement for 8 kA at room temperature.....	28
Figure 15 A waveform measurement for 10 kA at room temperature.....	28
Figure 16 A waveform measurement for 5 kA at 77 K	29
Figure 17 A waveform measurement for 10 kA at 77 K	29

10. List of tables

Table 1: Superconducting materials and their transition temperatures..... 6

Table 2 High speed camera settings for the various measurement requirements..... 25

11. References

- [1] B. Graver, K. Zhang, and D. Rutherford, "CO 2 emissions from commercial aviation, 2018," 2018.
- [2] A. Cristea, D. Hummels, L. Puzzello, and M. Avetisyan, "Trade and the greenhouse gas emissions from international freight transport," *J Environ Econ Manage*, vol. 65, no. 1, pp. 153–173, 2013, doi: 10.1016/j.jeem.2012.06.002.
- [3] "U.S. Releases First-Ever Comprehensive Aviation Climate Action Plan to Achieve Net-Zero Emissions by 2050 | US Department of Transportation." <https://www.transportation.gov/briefing-room/us-releases-first-ever-comprehensive-aviation-climate-action-plan-achieve-net-zero> (accessed Jan. 31, 2022).
- [4] J. L. Felder, H. D. Kim, and G. v Brown, "Turboelectric Distributed Propulsion Engine Cycle Analysis for Hybrid-Wing-Body Aircraft."
- [5] H. D. Kim, A. T. Perry, and P. J. Ansell, "A Review of Distributed Electric Propulsion Concepts for Air Vehicle Technology," in *2018 AIAA/IEEE Electric Aircraft Technologies Symposium, EATS 2018*, Nov. 2018. doi: 10.2514/6.2018-4998.
- [6] J. S. Thongam, M. Tarbouchi, A. F. Okou, D. Bouchard, and R. Beguenane, "All-electric ships - A review of the present state of the art," in *2013 8th International Conference and Exhibition on Ecological Vehicles and Renewable Energies, EVER 2013*, 2013. doi: 10.1109/EVER.2013.6521626.
- [7] R. del Rosario, "A Future with Hybrid Electric Propulsion Systems: A NASA Perspective," *Turbine Engine Technology Symposium*, pp. 1–21, 2014, [Online]. Available: <https://ntrs.nasa.gov/search.jsp?R=20150000748>
- [8] J. L. Felder, "NASA N3-X with TeDP," *Fundamental Aeronautics Program*, 2012.
- [9] S. Pamidi, C. H. Kim, and L. Graber, "High-temperature superconducting (HTS) power cables cooled by helium gas," in *Superconductors in the Power Grid: Materials and Applications*, 2015, pp. 225–260. doi: 10.1016/B978-1-78242-029-3.00007-8.
- [10] N. H. Doerry and H. Fireman, "Designing All Electric Ships," *Proceedings of the Ninth International Marine Design Conference*, p. 475, 2006.
- [11] C. M. Rey and A. P. Malozemoff, "Fundamentals of superconductivity," in *Superconductors in the Power Grid*, Elsevier, 2015, pp. 29–73. doi: 10.1016/B978-1-78242-029-3.00002-9.
- [12] B. G. Marchionini, Y. Yamada, L. Martini, and H. Ohsaki, "High-Temperature Superconductivity: A Roadmap for Electric Power Sector Applications, 2015-2030," *IEEE Transactions on Applied Superconductivity*, vol. 27, no. 4, pp. 1–7, 2017, doi: 10.1109/TASC.2017.2671680.
- [13] N. Doerry and J. v. Amy, "Design considerations for a reference MVDC Power System," *Transactions - Society of Naval Architects and Marine Engineers*, vol. 124, no. November, pp. 40–59, 2016.

- [14] H. Kamerlingh Onnes, "Further Experiments with liquid Helium," *Leiden Communications*, vol. 120b, 122b, pp. 261–271, 1911.
- [15] A. P. Malozemoff, "The power grid and the impact of high-temperature superconductor technology: An overview," in *Superconductors in the Power Grid: Materials and Applications*, 2015. doi: 10.1016/B978-1-78242-029-3.00001-7.
- [16] C. M. Rey and A. P. Malozemoff, "Fundamentals of superconductivity," in *Superconductors in the Power Grid*, Elsevier, 2015, pp. 29–73. doi: 10.1016/B978-1-78242-029-3.00002-9.
- [17] A. Morandi, "HTS dc transmission and distribution: concepts, applications and benefits," *Supercond Sci Technol*, vol. 28, no. 12, p. 123001, 2015, doi: 10.1088/0953-2048/28/12/123001.
- [18] S. P. Transmission, P. J. Ferrara, M. A. Uva, J. Nowlin, and A. P. Side, "Naval Ship-to-Shore High Temperature," vol. 21, no. 3, pp. 984–987, 2011.
- [19] P. Cheetham, "Investigation of Alternative Cryogenic Dielectric Materials and Designs for High Temperature Superconducting Devices," 2017. [Online]. Available: <http://fsu.digital.flvc.org/islandora/object/fsu%3A552044%0Ahttps://search.proquest.com/docview/1985130664?accountid=4840>
- [20] L. Graber *et al.*, "Grounding of Shipboard Power Systems - Results from Research and Preliminary Guidelines for the Shipbuilding Industry," 2014. [Online]. Available: <https://esrdc.com/library/?q=node/704>
- [21] J. F. Maguire *et al.*, "Program update on the development and demonstration of a HTS power cable to operate in the long Island power authority transmission grid," *2007 IEEE Power Engineering Society General Meeting, PES*, vol. 17, no. 2, pp. 2034–2037, 2007, doi: 10.1109/PES.2007.386203.
- [22] J. X. Jin *et al.*, "Enabling high-temperature superconducting technologies toward practical applications," *IEEE Transactions on Applied Superconductivity*, vol. 24, no. 5, 2014, doi: 10.1109/TASC.2014.2346496.
- [23] M. Stemmler, F. Merschel, M. Noe, and A. Hobl, "AmpaCity - Advanced superconducting medium voltage system for urban area power supply," *Proceedings of the IEEE Power Engineering Society Transmission and Distribution Conference*, pp. 1–5, 2014, doi: 10.1109/tdc.2014.6863566.
- [24] T. Masuda *et al.*, "A new HTS cable project in Japan," *IEEE Transactions on Applied Superconductivity*, vol. 19, no. 3, pp. 1735–1739, 2009, doi: 10.1109/TASC.2009.2018157.
- [25] J. A. Demko *et al.*, "Triaxial HTS cable for the AEP bixby project," *IEEE Transactions on Applied Superconductivity*, vol. 17, no. 2, pp. 2047–2050, 2007, doi: 10.1109/TASC.2007.897842.
- [26] N. Hayakawa *et al.*, "Dielectric characteristics of HTS cables based on partial discharge measurement," *IEEE Transactions on Applied Superconductivity*, vol. 15, no. 2 PART II, pp. 1802–1805, 2005, doi: 10.1109/TASC.2005.849292.

- [27] C. H. Kim, J. Kim, and S. v Pamidi, "Cryogenic Thermal Studies on Cryocooler-Based Helium Circulation System for Gas Cooled Superconducting Power Devices," *International Cryocooler Conference*, pp. 504–513, 2014.
- [28] C. H. Kim, S. K. Kim, L. Graber, and S. v. Pamidi, "Cryogenic thermal studies on terminations for helium gas cooled superconducting cables," *Phys Procedia*, vol. 67, pp. 201–207, 2015, doi: 10.1016/j.phpro.2015.06.035.
- [29] L. Graber, C. H. Kim, S. v Pamidi, and D. Knoll, "Dielectric Design Validation of a Helium Gas Cooled Superconducting DC Power Cable," no. June, pp. 157–161, 2014.
- [30] P. Cheetham, W. Kim, C. H. Kim, S. v. Pamidi, L. Graber, and H. Rodrigo, "Use of partial discharge inception voltage measurements to design a gaseous helium cooled high temperature superconducting power cable," *IEEE Transactions on Dielectrics and Electrical Insulation*, vol. 24, no. 1, pp. 191–199, 2017, doi: 10.1109/TDEI.2016.005909.
- [31] N. Kelley, M. Nassi, and L. Masur, "Application of HTS wire and cables to power transmission: State of the art and opportunities," *Proceedings of the IEEE Power Engineering Society Transmission and Distribution Conference*, vol. 2, no. WINTER MEETING, pp. 448–454, 2001, doi: 10.1109/pesw.2001.916883.
- [32] J. Gerhold and T. Tanaka, "Cryogenic electrical insulation of superconducting power transmission lines: Transfer of experience learned from metal superconductors to high critical temperature superconductors," *Cryogenics (Guildf)*, vol. 38, no. 11, pp. 1173–1188, 1998, doi: 10.1016/S0011-2275(98)00105-2.
- [33] M. Yazdani-Asrami, S. Seyyedbarzegar, A. Sadeghi, W. T. B. de Sousa, and D. Kottonau, "High temperature superconducting cables and their performance against short circuit faults: Current development, challenges, solutions, and future trends," *Supercond Sci Technol*, vol. 35, no. 8, Aug. 2022, doi: 10.1088/1361-6668/ac7ae2.
- [34] L. Xiao, S. Dai, L. Lin, Z. Zhang, and J. Zhang, "HTS power technology for future dc power grid," *IEEE Transactions on Applied Superconductivity*, vol. 23, no. 3, 2013, doi: 10.1109/TASC.2013.2238972.
- [35] J. F. Maguire *et al.*, "Progress and status of a 2G HTS power cable to be installed in the Long Island Power Authority (LIPA) grid," *IEEE Transactions on Applied Superconductivity*, vol. 21, no. 3 PART 2, pp. 961–966, 2011, doi: 10.1109/TASC.2010.2093108.
- [36] J. T. Kephart, B. K. Fitzpatrick, P. Ferrara, M. Pyryt, J. Pienkos, and E. Michael Golda, "High temperature superconducting degaussing from feasibility study to fleet adoption," *IEEE Transactions on Applied Superconductivity*, vol. 21, no. 3 PART 2, pp. 2229–2232, 2011, doi: 10.1109/TASC.2010.2092746.
- [37] B. K. Fitzpatrick, J. T. Kephart, and E. Michael Golda, "Characterization of gaseous helium flow cryogen in a flexible cryostat for naval applications of high temperature superconductors," *IEEE Transactions on Applied Superconductivity*, vol. 17, no. 2, pp. 1752–1755, 2007, doi: 10.1109/TASC.2007.897763.

- [38] H. Rodrigo, D. Kwag, L. Graber, B. Trociewitz, and S. Pamidi, "AC flashover voltages along epoxy surfaces in gaseous helium compared to liquid nitrogen and transformer oil," *IEEE Transactions on Applied Superconductivity*, vol. 24, no. 3, pp. 3–8, 2014, doi: 10.1109/TASC.2013.2286744.
- [39] L. Jin, C. Lee, S. Baek, and S. Jeong, "Design of high-efficiency Joule-Thomson cycles for high-temperature superconductor power cable cooling," *Cryogenics (Guildf)*, 2018, doi: 10.1016/j.cryogenics.2018.05.003.
- [40] M. Hazezama, T. Kobayashi, N. Hayakawa, S. Honjo, T. Masuda, and H. Okubo, "Partial discharge inception characteristics under butt gap condition in liquid nitrogen/PPLP® composite insulation system for high temperature superconducting cable," *IEEE Transactions on Dielectrics and Electrical Insulation*, vol. 9, no. 6, pp. 939–944, 2002, doi: 10.1109/TDEI.2002.1115487.
- [41] P. Cheetham, C. H. Kim, L. Graber, and S. Pamidi, "Practical Considerations for the Design of a Superconducting Gas-Insulated Transmission Line for Shipboard Applications," *IEEE Electrical Ship Technical Symposium*, 2017.
- [42] P. Cheetham *et al.*, "High Temperature Superconducting Power Cables for MVDC Power Systems of Navy Ships".
- [43] P. Cheetham, W. Kim, C. H. Kim, L. Graber, H. Rodrigo, and S. Pamidi, "Enhancement of Dielectric Strength of Cryogenic Gaseous Helium by Addition of Small Mol% Hydrogen," *IEEE Transactions on Applied Superconductivity*, vol. 27, no. 4, pp. 1–5, Jun. 2017, doi: 10.1109/TASC.2016.2642539.
- [44] L. Graber, W. J. Kim, P. Cheetham, C. H. Kim, H. Rodrigo, and S. v Pamidi, "Dielectric Properties of Cryogenic Gas Mixtures Containing Helium, Neon, and Hydrogen," *IOP Conf Ser Mater Sci Eng*, vol. 102, p. 012018, 2015, doi: 10.1088/1757-899X/102/1/012018.
- [45] C. Park, S. Pamidi, and L. Graber, "The critical electric field of gas mixtures over the extended range of cryogenic operating conditions," *J Appl Phys*, vol. 122, no. 15, 2017, doi: 10.1063/1.4995663.
- [46] P. Cheetham, C. H. Kim, L. Graber, and S. Pamidi, "Practical Considerations for the Design of a Superconducting Gas-Insulated Transmission Line for Shipboard Applications," *IEEE Electrical Ship Technical Symposium*, 2017.
- [47] S. G. P. Cable *et al.*, "Development of a High-Temperature," vol. 30, no. 6, 2020.
- [48] P. Cheetham, C. H. Kim, S. Pamidi, and L. Graber, "Optimization of a superconducting gas-insulated transmission line," *IEEE Transactions on Dielectrics and Electrical Insulation*, vol. 26, no. 3, pp. 930–938, 2019, doi: 10.1109/tdei.2019.007884.
- [49] P. Cheetham, S. Telikapalli, T. Stamm, C. H. Kim, and S. V. Pamidi, "HTS Technology Driven Shipboard Power Distribution Architecture-Electrical," *2021 IEEE Electric Ship Technologies Symposium, ESTS 2021*, pp. 2–7, 2021, doi: 10.1109/ESTS49166.2021.9512331.
- [50] P. Cheetham, S. Telikapalli, T. Stamm, C. H. Kim, and S. v. Pamidi, "HTS Technology Driven Shipboard Power Distribution Architecture-Electrical," *2021 IEEE Electric Ship Technologies Symposium, ESTS 2021*, 2021, doi: 10.1109/ESTS49166.2021.9512331.

- [51] T. Stamm *et al.*, "Electrical faults in high temperature superconducting power cables for MVDC power systems of all-electric ships," in *IOP Conference Series: Materials Science and Engineering*, Jun. 2020, vol. 755, no. 1. doi: 10.1088/1757-899X/755/1/012135.